Research on Engineering Structures & Materials
journal homepage: http://www.jresm.org
Research Group

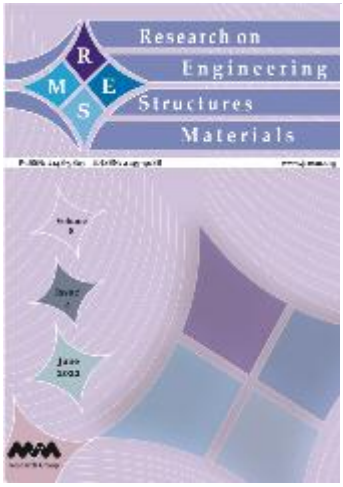

Nonlinear coupled thermal-structural analysis of precast concrete beam-to-column connections at high temperatures

Noor Azim Mohd. Radzi, Muhaimim Kamal, Shareen Azuha, Nur Izzatie Aqilah Mansor, Roszilah Hamide

Online Publication Date: 20 April 2023
URL: http://www.jresm.org/archive/resm2023.610ma1220.html
DOI: http://dx.doi.org/10.17515/resm2023.610ma1220
Journal Abbreviation: *Res. Eng. Struct. Mater.*

To cite this article
Radzi NAM, Kamal M, Azuha S, Mansor NIA, Hamide R. Nonlinear coupled thermal-structural analysis of precast concrete beam-to-column connections at high temperatures. *Res. Eng. Struct. Mater.*, 2023; 9(3): 969-987.

Research on Engineering Structures & Materials
journal homepage: http://www.jresm.org
Research Group

Research Article

Nonlinear coupled thermal-structural analysis of precast concrete beam-to-column connections at high temperatures

Noor Azim Mohd. Radzi[*,a], Muhaimim Kamal[b], Shareen Azuha[c], Nur Izzatie Aqilah Mansor[d], Roszilah Hamid[e]

Department of Civil Engineering, Universiti Kebangsaan Malaysia, Selangor D. E., Malaysia

Article Info

Article history:

Received 20 Dec 2022
Accepted 18 Apr 2023

Keywords:

Finite element analysis; Fire resistance; Beam-to-column connections; Thermal response

Abstract

This paper presents a nonlinear coupled thermal-structural analysis using ANSYS Workbench to determine precast beam-to-column connections' thermal and structural behaviour. Three precast connection models, a concrete corbel, a concrete nib, and an inverted E steel nib, are exposed to ambient and cellulose fire curves. Firstly, the precast connection models are verified based on the previous experimental result at ambient temperature. Then, the verified precast connection models are exposed to the cellulose fire curve for two hours before being loaded to failure. The results are compared with the recent experimental fire test conducted by the authors. Based on the result, finite element models at ambient temperature were validated with a percentage difference of less than 10%. However, finite element models at high temperatures were not verified due to the percentage difference exceeding 10 %. The significant difference was due to the non-uniformity of sample dimensions and different test setups in the previous experiment. Finite element models for concrete corbel and inverted E steel nib have a higher stiffness than the experimental sample. However, the finite element model for concrete nib has a lower stiffness than the experimental sample. Concrete nib recorded the most significant thermal percentage deterioration (32.1 % and 57.4 %) compared to concrete corbel (22.4 % and 11.52 %) and inverted E steel nib (26.9 % and 27.9 %). The validation result of nonlinear coupled thermal-structural analysis executed using ANSYS Workbench gives good efficiency for predicting the fire performance of precast concrete corbel beam-to-column connections at high temperatures.

1. Introduction and Objectives

Precast concrete technology is widely used around the world. The various advantages of precast concrete make it the leading choice in construction materials today. Prefabrication of concrete on structural components outside the construction site during construction will reduce the period and use of materials, thus saving costs compared to conventional construction methods (1). Precast structures contain complex precast concrete connections that contribute to the overall structure (2). Precast beam-to-column connections are one of the structural elements that are important in improving structures' behaviour. Concrete corbel and concrete nib are the most used type in precast construction. They transfer vertical loads from the beam to the columns. In addition, a new method of hybrid connection was introduced, such as an inverted E steel nib (3).

According to Eurocodes (4), fire is classified as an accidental load that must be considered in the structural design process. The connection's behaviour of precast concrete exposed to fire or high temperatures is determined by complex interactions during the heating

[*]Corresponding author: p100973@siswa.ukm.edu.my
[a] orcid.org/0000-0003-4017-7735; [b] orcid.org/0000-0002-7389-4338, [c] orcid.org/0000-0003-1665-0393, [d] orcid.org/0000-0001-9306-4481, [e]orcid.org/0000-0002-4617-970X
DOI: http://dx.doi.org/10.17515/resm2023.610ma1220

process and depends on the composition of the mixture (5–7). When exposed to fire, the failure mode of precast concrete connection is distinguished by fire type or temperature, load system and structure. Teja (8) stated that post-fire effects on connection elements in precast structures, such as bearing, pavement, and welding, also influence moment-rotation characteristics. Fire-damaged to beam-to-column connections also reduces the rigidity of the beam structure and the integrity between the beam end and the column face, reducing the toughness of the connection. The ASTM E119 (9) and ISO 834 (10) methods provided the standard test to identify the response of structures and materials to fire. The behaviour of structural members is analysed and measured according to the period of resistance to the fire load. However, the methods focus on the individual structural members, not the structural subassembly, including beam-to-column connections. The response can only be observed and analysed in vertical structural members such as columns, walls, and dividers and transverse structural members such as beams and slabs.

Literature shows that the fire test study on the precast beam-to-column connection at high temperatures is limited compared to the study on monolithic and steel connection (11,12). An experimental study by Teja (8) on three types of precast beam-to-column connections at high temperatures only made against a temperature of 400 °C, which is too low compared to the maximum cellulose fire curve temperature (1057 °C). Radzi (13) has performed a fire test of a precast beam-to-column connection at a cellulose fire curve to overcome this gap. The test involves two types of connections commonly used in precast building construction: concrete corbel and concrete nib, and a new connection type inverted E steel nib (3). A comparison was made with the result at ambient temperature on the load-deflection and moment-rotation curves.

The use of computer software aims to simplify the calculation of complex structural analysis and can save time. Finite element simulation using computer software can perform analysis for various engineering problems. Computer software such as ABAQUS, VULCAN, ADAPTIC, DIANA, and ANSYS can be used in transient structural analysis and coupled thermal structural analysis of beam-to-column connections (14–16). Finite element simulations can confirm experimental findings, predict thermal and structural behaviour using different parameters, and improve engineering recommendations. Considerations are made based on thermal and structural constraints, thermal and structural loads, and material properties.

In this paper, a nonlinear coupled thermal-structural analysis is executed using ANSYS Workbench to determine the thermal and structural behaviour of precast beam-to-column connections (concrete corbel, concrete nib, and an inverted E steel nib) exposed to ambient and cellulose fire curve. Firstly, the finite element models are verified based on the previous experimental test result at ambient temperature (3,17,18). Since the previous experiment (3,17,18) were not made for high temperature, the comparison of the finite element simulation at high temperature was made with the experiment by Radzi (13). The study's findings are presented as load-deflection and moment-rotation curves. Finally, the thermal percentage deterioration of the connection summarised the best connection with fire resistance capability at high temperatures.

2. Description of Specimens at Ambient Temperature

This study adopted the experimental test results at ambient temperature by Abd. Rahman et al. (17) for the concrete corbel model, Mokhtar et al. (18) for the concrete nib, and Bahrami et al. (3) for the inverted E steel nib. The test setup, detail of the test specimen, material properties, and test procedure are summarised in this section. More details of this experiment can be found in the paper (3,17,18).

2.1 Concrete Corbel

The sizes of the concrete corbel components, beams and columns are shown in Fig. 1. The size of the precast beam is 160 mm x 280 mm, while the size of the precast column is 200 mm x 200 mm. Table 1 lists the concrete corbel connection's reinforcement and concrete cover details. Half-depth precast beams were installed on both sides of the corbels, followed by the installation of 2Y16 top reinforcement bars, while 2Y16 of the bottom reinforcement bars were already cast in the half beam. A second stage of concreting using wet cast-in-place concrete was carried out using simple side formwork along the beam to complete the connection between the precast beam and precast column.

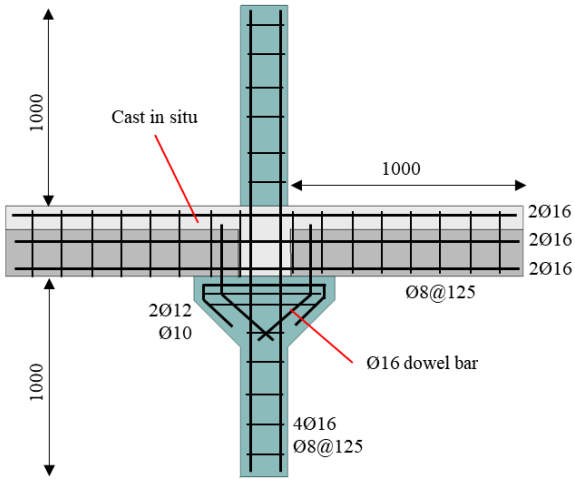

Fig. 1 Concrete corbel connection detailing (17)

Table 1. Reinforcement and concrete cover detailing (17)

Items	Descriptions
Top and bottom steel bar beam	2Y16
Stirrup beam	R8-125
Main bar column	4Y16
Stirrup column	R8-125
Dowel bar	Y16
Concrete cover of column and corbel	25mm
Concrete cover of beam	25mm

2.2 Concrete Nib

The sizes of the concrete nib components, beams and columns are shown in Fig. 2. The beam size is 300 mm × 450 mm and 1500 mm long. The column is 300 mm × 300 mm, with a total height of 3000 mm and a cross-section containing four T25 mm rebars. The tension reinforcements are fully anchored and lapped to ensure that full tensile force can be developed at this connection without slippage or failure. Flexural reinforcements were anchored inside the columns with a 90° bend. The connection used two 20 mm high-yield deformed bars as top reinforcement. The precast components' compressive strength, fcu, at 28 days was 40 N/mm2. The compressive strength of the infill concrete mix, fcui, was designed to be 40 N/mm2 in 7 days.

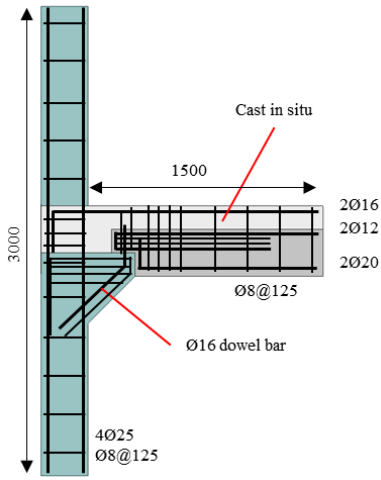

Fig. 2 Concrete nib connection detailing (18)

2.3 Inverted E Steel Nib

The sizes of the inverted E steel nib components, beams and columns are shown in Fig. 3. The beam size is 250 mm × 320 mm and 1376 mm long. The column is 250 mm × 250 mm, with a total height of 1500 mm. The precast concrete beam is placed on the embedded steel corbel in the continuous column, and the bottom threaded bars of the beam are tightened between the grooves of the corbel by two nuts and steel gaskets with a thickness of 10 mm. The space of the connection area is filled with expandable grout. After grouting, two top bars were passed through two holes in the column. Those holes are also grouted, and the connection is completed by slab concreting.

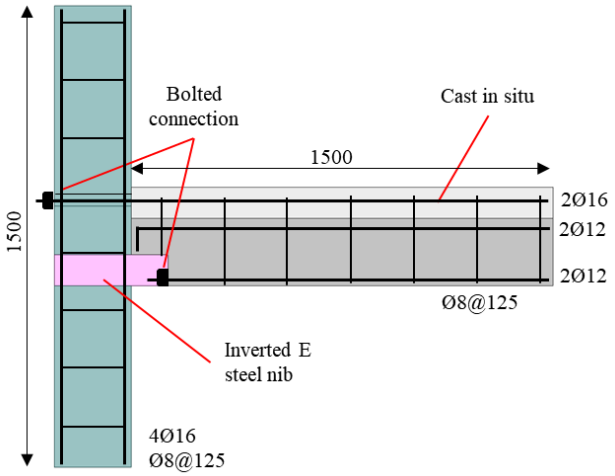

Fig. 3 Inverted E steel nib connection detailing (3)

3. Previous Study at High Temperature

Radzi (13) studied the behaviour of precast concrete beam-to-column connections subjected to standard cellulose fire exposure, as shown in Fig. 4. The behaviour of precast concrete beams to column connection specimens, namely concrete corbel, concrete nib, and inverted E steel nib, were compared with monolithic type specimens. The specimens were produced based on the IBS catalogue produced by the Public Works Department of Malaysia (JKR) and the Construction Industry Development Board of Malaysia (CIDB). The dimensions and test setup used were not uniform in this study. However, the test results by Radzi (13) can still be used as a reference for comparison purposes.

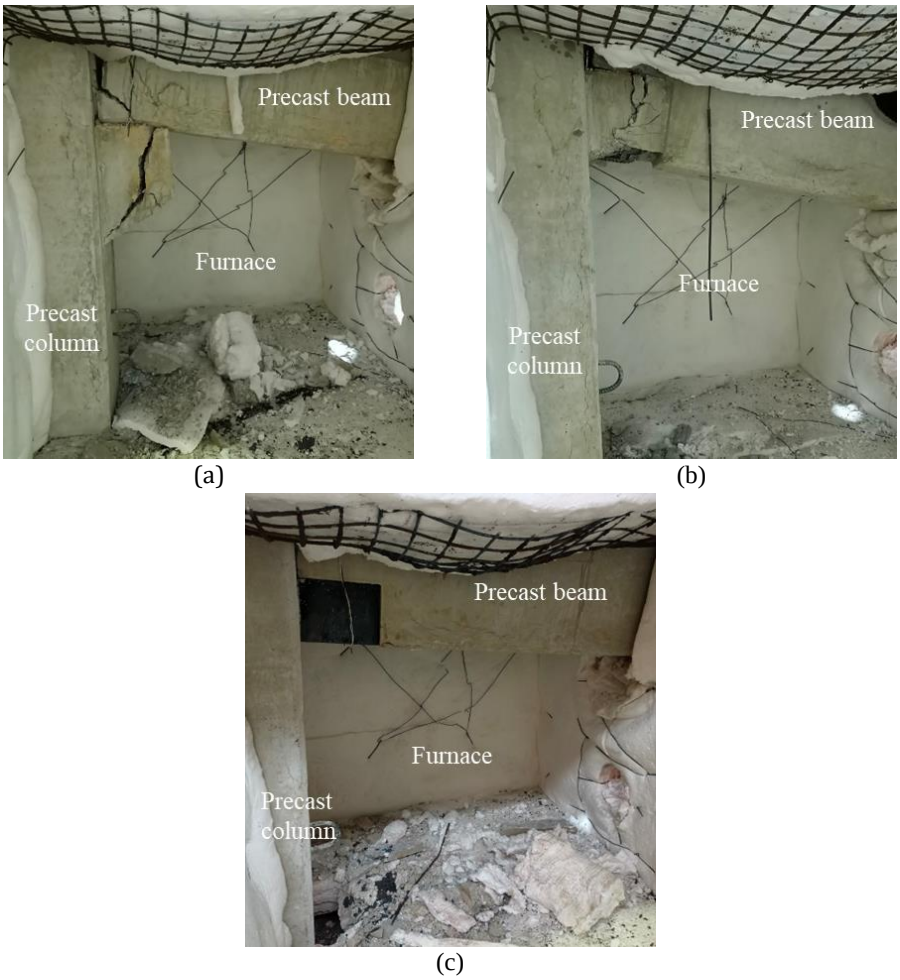

Fig. 4 Fire damaged of precast concrete beam to column connections: (a) concrete corbel, (b) concrete nib, and (c) inverted E steel nib (13).

4. Numerical Models

4.1 Finite Element Models

The details of the finite element models are given in Table 2. A total of six finite element models are provided, three for ambient temperature and three more for high temperature.

For the finite element model references, the first letter CC, CN, and EN stands for concrete corbel, concrete nib, and Inverted E steel nib, respectively, while the following letter A and HT represents the ambient and high temperature conditions. The geometric modelling was executed using additional software, SpaceClaim 2021 R2. Fig. 5 shows the geometric models produced: concrete corbel, concrete nib, and inverted E steel nib. The geometry of concrete, grout, rubber pads, and steel plates as volumes were produced by solid modelling methods. In contrast, the geometry of the steel reinforcement was produced as a line using the direct generation method. Convergence analysis subjected to an increasing static load at the end of the beam until the connection fails was done on five different mesh sizes of the beam to monolithic column connection model. The sizes were 125 mm, 100 mm, 75 mm, 50 mm, and 25 mm. The deflection values for the 50 mm and 25 mm mesh sizes show a lower gradient with a consistent deflection difference of only 0.5 mm. Because the small mesh size (25 mm) will affect the duration of the simulation solution, this thesis chooses a more appropriate and reasonable mesh size of 50 mm based on the size of the large-scale model and requires a suitable period to complete. The chosen type of mesh was linear and hexahedral in shape with six surfaces.

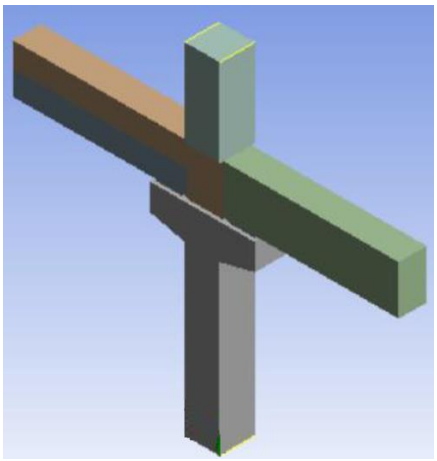

(a)

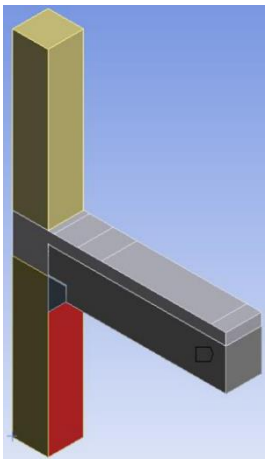

(b)

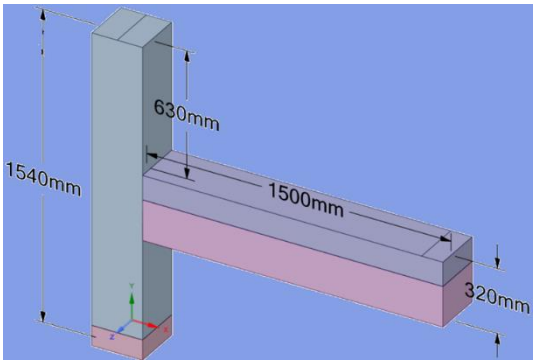

(c)

Fig. 5 Geometric modelling: (a) concrete corbel, (b) concrete nib, and (c) inverted E steel nib

Table 2. Details of finite element models at ambient temperature

Conditions	Connections	Finite Element Model References
Ambient	Concrete corbel (17)	CC-A
	Concrete nib (18)	CN-A
	Inverted E steel nib (3)	EN-A
High Temperature	Concrete corbel (17)	CC-HT
	Concrete nib (18)	CN-HT
	Inverted E steel nib (3)	EN-HT

4.2 Simulation Procedures

The nonlinear coupled thermal-structural analysis using ANSYS Workbench was performed to validate the experimental result and predict the behaviour under different parameters (19). This sequential coupling technique was chosen to connect thermal and structural analysis. The simulation procedures inside the ANSYS program are illustrated in Fig. 6. In Step 1, the transient structural analysis was executed. The material properties at ambient temperature and structural boundary conditions were assigned to the model.

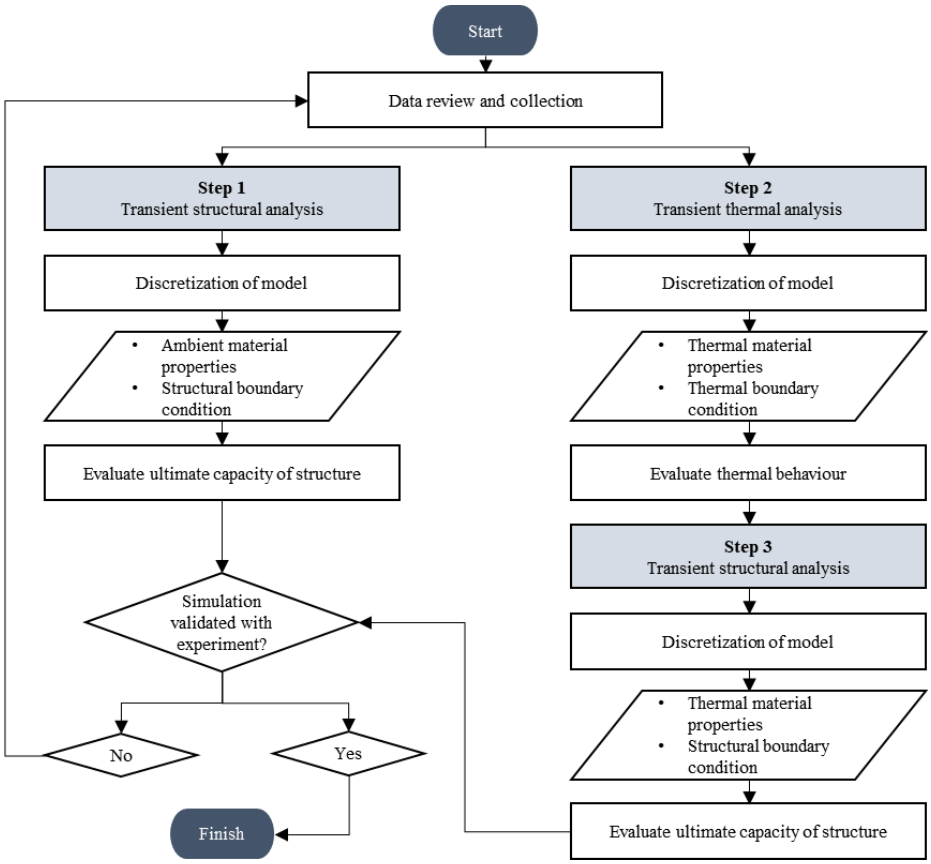

Fig. 6 Fire Finite element simulation procedures

The gradual load was applied to the end of the beam to allow for beam failure. Then, the ultimate capacity of the structure at ambient temperature was evaluated. In Steps 2 and 3, The transient thermal and structural analyses were executed. Transient thermal analysis

was performed first and followed by transient structural analysis. The temperature-dependent thermal properties and thermal boundary conditions were assigned to the model. The cellulose fire curve temperature profile was applied to the model. The temperature solution at a high temperature was evaluated. Then, the computed temperature solution was used as input data to determine the deformation and thermal stress of the structure at high temperatures.

Mesh studies are performed to determine the optimal finite element mesh, which provides a relatively accurate solution method with low calculation time. This section divides the large structure into small parts to facilitate analysis. The optimal size and short analysis period were used in this study. Trial-and-error methods for different sizes determine the optimal mesh size. In this analysis, the selected mesh size is 25 mm (for concrete nib) and 50 mm (for concrete corbel and inverted E steel nib) because it shows reasonable force convergence (Force Convergence). This value is adapted for all model components, such as concrete, reinforcement bar and stirrups. The fixed support was assigned at the top and bottom of the precast concrete column. The interface between rebar elements and concrete was assumed to be fully bonded using the discrete reinforcing method. The explosive spalling phenomena on the concrete surface during heating were neglected.

4.3 Thermal and Structural Elements

The element characteristics were described by ANSYS (20). For transient thermal analysis, SOLID278 was assigned to simulate the concrete element. SOLID278 has a 3-D thermal conduction capability. The element has eight nodes with a single degree of freedom and temperature at each node. For transient structural analysis, SOLID278 was replaced by SOLID185 to simulate the concrete element. SOLID185 was selected for or the 3-D modelling of solid structures. Eight nodes define it with three degrees of freedom at each node: translations in the directions of the nodal x, y, and z. The element has plasticity, hyper elasticity, stress stiffening, creep, large deflection, and large strain capabilities. REINF264 was assigned for the transient thermal and transient structural analysis to reinforce the elements. REINF264 has plasticity, stress stiffening, creep, large deflection, and large strain capabilities.

4.4 Materials Properties

Table 3 lists the properties of the material used in ANSYS. The thermal and mechanical material properties assigned in the simulation were according to Eurocode (4) and previous studies (21,22).

Table 3. Materials properties

Properties	Concrete	Steel
Density (Kg mm^{-3})	2.3×10^{-6}	7.8×10^{-7}
Young's modulus (MPa)	35000	2×10^{5}
Poisson ratio	0.2	0.3
Bulk modulus	19444	1.63×10^{5}
Shear modulus (MPa)	14583	77160
Coefficient of thermal expansion (C^{-1})	1.48×10^{-5}	1.6×10^{-5}
Thermal conductivity (W mm-1 C^{-1})	0.002	0.054
Specific heat (mJ Kg^{-1} C^{-1})	9×10^{5}	4.8×10^{5}

The isotropic thermal conductivity and specific heat constant pressure vary with temperature. The density, isotropic elasticity (Young's modulus and Poisson's ratio),

multilinear isotropic hardening of concrete (plastic stress-strain), and bilinear isotropic hardening of reinforcement (yield strength-tangent modulus) are varied with respect to temperature.

4.5 Process of Data Analysis

The results obtained from the experimental and simulation were load-deflection and moment-rotation curves. For the simulation result using ANSYS, the load-deflection curves were directly obtained from a combined force and total deformation appeared in the graph and tabular data, as shown in Fig. 7 (a). For the experiment, the load-deflection curves were generated based on the applied load and the vertical directional deformation data at the end of the beam, as shown in Fig. 7 (b).

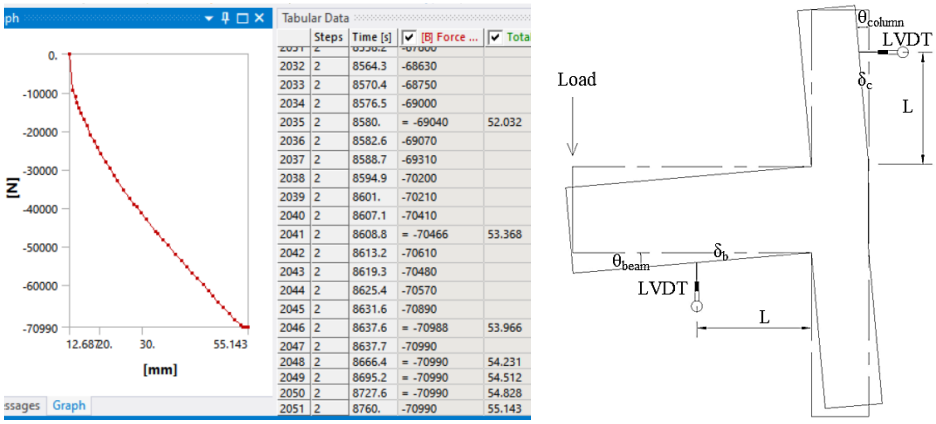

(a) (b)

Fig. 7 Load-deflection of connections: (a) results from ANSYS and (b) experimental relationship between deflection, δ and rotation, θ

From the load result, the moment (M) was calculated according to equation (1).

$$M = (F \times d) + \left(SW_b \times \frac{d}{2}\right) \quad (1)$$

where F is the applied force (in kN), d is the distance from the fixed axis (in mm), and SW_b is the selfweight of the beam (in kN). The rotation (θ) was calculated based on the difference between the rotation in the beam (θbeam) and the rotation in the column (θcolumn) according to equation (2).

$$\theta = \left\{\left[\tan^{-1}\frac{b}{d}\right] - \left[\tan^{-1}\frac{a}{c}\right]\right\} 100\pi/18 \quad (2)$$

where a is the deflection in the column (in mm), b is the deflection in the beam (in mm), c is the distance of the LVDT to the center of rotation of the column (in mm), and d is the distance of the LVDT to the center of rotation of the beam (in mm).

5. Results and Discussions

5.1 Concrete Corbel

5.1.1 Ambient Temperature

For model validation, Fig. 8 compares the load-deflection curves of model CC-A and the experiment by Abd. Rahman et al. (17) at ambient temperature. It is observed that the curves showed a good agreement between them. The deflection for the experiment was

45.7 mm with a maximum load of 62.4 kN. The deflection for model CC-A was 47.6 mm with a maximum load of 67 kN. The percentage difference for deflection and load was 4 % and 6.8 %, which validated the finite element model. Fig. 9 shows the moment–rotation curves of model CC-A and the experiment by Abd. Rahman (17) at ambient temperature. At the beginning of loading, there was a difference in the load value between the two curves. Model CC-A had a higher stiffness compared to the experiment. At load 67 kN, the curves showed a good agreement between them. The percentage difference for moment and rotation was 9.2 % and 7.7 %, respectively.

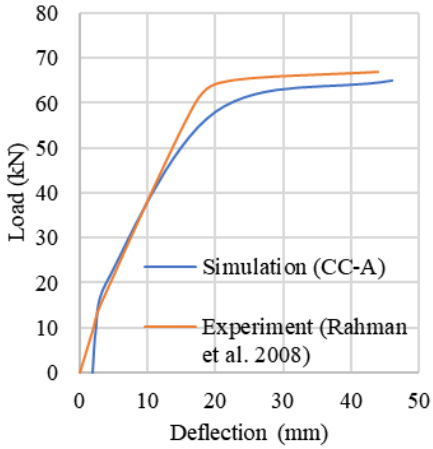

Fig. 8 Load – deflection curves of model CC-A and experiment (17) at ambient temperature

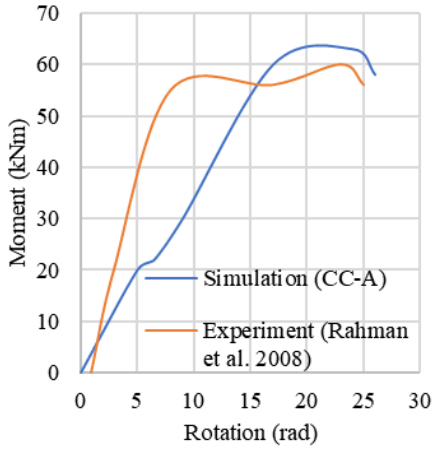

Fig. 9 Moment – rotation curves of model CC-A and experiment (17) at ambient temperature

5.1.2 High Temperature

For model validation, Fig. 10 shows the load-deflection curves of model CC-HT and the experiment by Radzi (13)at high temperatures. It is observed that there was a difference in the load value of 10 kN between the two curves. This is due to the non-uniformity of sample dimensions and different test setups in the study by Radzi (2023) (13), which was not considered in the simulation. A constant load of 10 kN was applied to the sample during the experiment. Table 4 compares the load–deflection ratio between the model CC-HT and the experiment by Radzi (13). The load–deflection ratio showed a good agreement between them, with a slight difference of 6.1%.

Table 4. Load – deflection ratio between CC-HT and experiment [9] at high temperature

Items	CC-HT [A]	Experiment (13) [B]	Differences [B] – [A]	Percentage Difference (%)
Load (kN)	52.39	60	7.61	12.68
Deflection (mm)	52.43	64.66	12.23	18.91

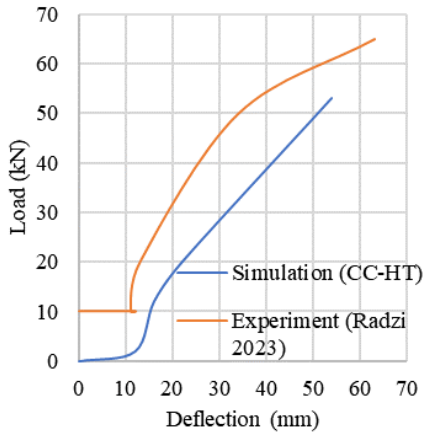

Fig. 10 Load – deflection curves of model CC-HT and experiment [9] at high temperature

5.1.3 Comparison of Ambient and High Temperature

Fig. 11 illustrates the deflection of model CC-A at ambient temperature and model CC-HT at high temperature. The comparison between these two results is important to determine the effect of the term on the model after being loaded at high temperature. The maximum deflection for model CC-A was 47.6 mm, with a maximum load of 67 kN. The maximum deflection for model CC-HT was 53.8 mm, with a maximum load of 52 kN. Observation showed that CC-A was performing better than CC-HT. Even though the deflection at ambient temperature is high, the maximum load is lower compared to the high temperature. Model CC-A had a higher stiffness compared to the CC-HT. The thermal percentage deterioration of load and displacement is 22.4 % and 11.52 %, respectively.

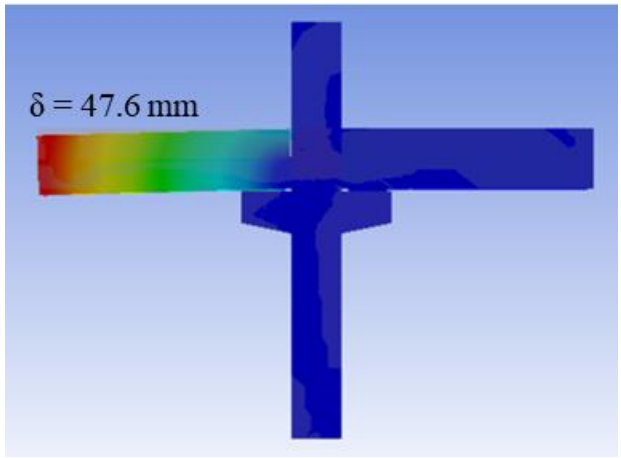

(a)

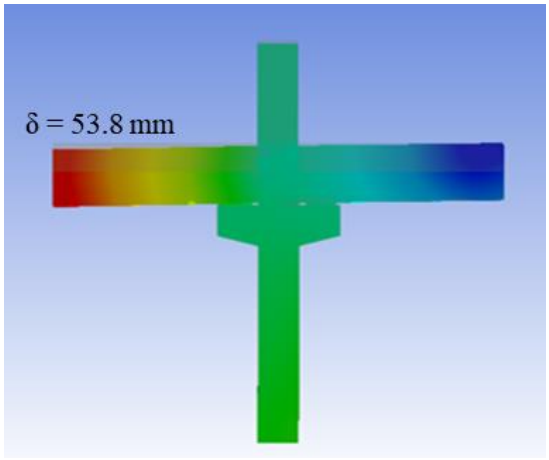

(b)

Fig. 11 Deflection of connection: (a) Model CC-A and (b) Model CC-HT

5.2 Concrete Nib

5.2.1 Ambient Temperature

For model validation, Fig. 12 and Fig. 13 show the deflection of model CN-A and load-deflection curves of model CN-A and the experimental test by Mokhtar et al. (18) at ambient temperature, respectively. It is observed that the curves showed a good agreement between them. In the experimental test, the deflection recorded was 8.33 mm with a maximum load of 60 kN. The deflection recorded in the simulation was 9 mm with a maximum load of 60 kN. The percentage difference for deflection was 7.8%, which validated the finite element model. Fig. 14 shows the moment–rotation curves of model CN-A and the experiment by Mokhtar et al. (18) at ambient temperature. It is observed that the curves showed a good agreement between them. The experiment specimen had a higher stiffness compared to the model CN-A. The percentage difference for rotation was 8.9%.

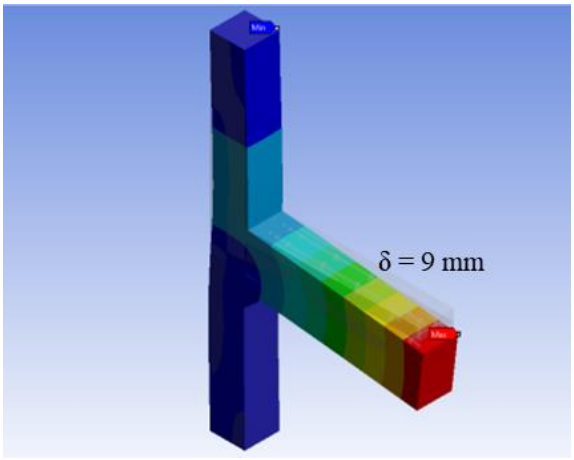

Fig. 12 Deflection of connection for model CN-A

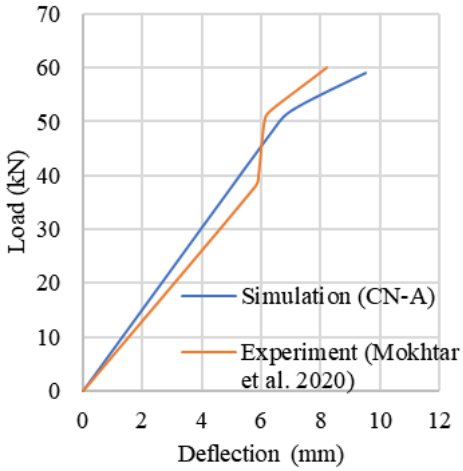

Fig. 13 Load – deflection curves of model CN-A and experiment [12] at ambient temperature

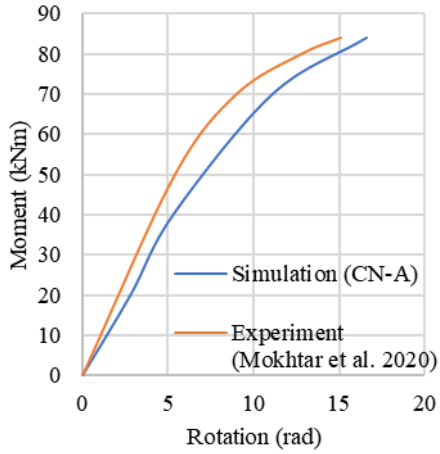

Fig. 14 Moment - rotation curves of model CN-A and experiment [12] at ambient temperature

5.2.2 High temperature

For model validation, Fig. 15 shows the load-deflection curves of model CN-HT and the experiment by Radzi (13) at high temperatures. Table 5 compares the load–deflection ratio between the model CN-HT and the experiment by Radzi (13). The load–deflection ratio showed a difference of 29.3%. This significant difference was due to the non-uniformity of sample dimensions and different test setups in the study by Radzi (2023) (13). The load in the simulation was a lateral applied at the column. The load in the experiment was vertical and applied to the beam.

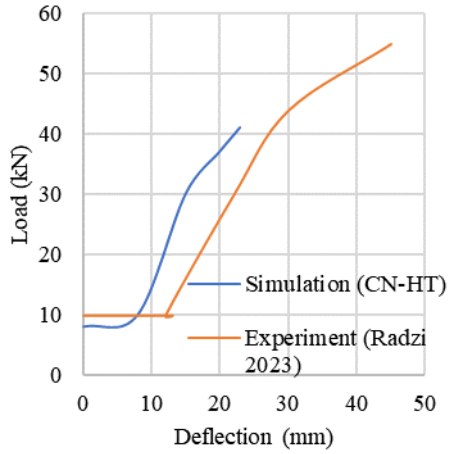

Fig. 15 Load – deflection curves of model CN-HT and experiment [9] at high temperature

Table 5. Load – deflection curves of model CN-HT and experiment (13) at high temperature

Items	CN-HT [A]	Experiment (13) [B]	Differences [B] – [A]	Percentage Difference (%)
Load (kN)	40.70	56.47	15.77	27.9
Deflection (mm)	22.93	45.26	22.33	49.34

5.2.3 Comparison of Ambient and High Temperature

Fig. 16 shows the load-deflection curves of models CN-A and CN-HT. The maximum deflection for model CN-A was 9.76 mm with a maximum load of 60 kN. The maximum deflection for model CN-HT was 22.93 mm with a maximum load of 40.7 kN. Observation showed that CN-A was performing better than CN-HT. The thermal percentage deterioration of load and displacement is 32.1 % and 57.4 %, respectively.

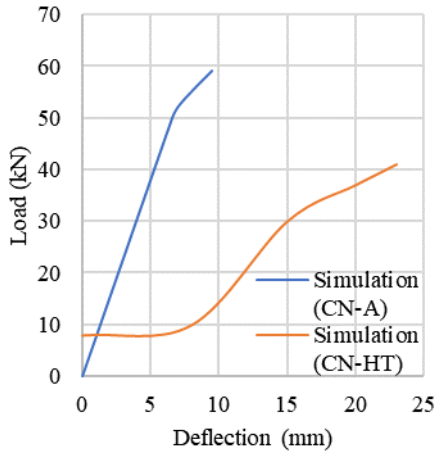

Fig. 16 Load – deflection curves of model CN-A and CN-HT

5.3 Inverted E Steel Nib

5.3.1 Ambient Temperature

For model validation, Fig. 17 and Fig. 18 show the deflection of model EN-A and load-deflection curves of model EN-A and the experimental test by Bahrami et al. (3) at ambient temperature, respectively. It is observed that the curves showed a good agreement between them. In the experimental test, the deflection recorded was 43 mm with a maximum load of 130 kN. The deflection recorded in the simulation was 39 mm with a maximum load of 130 kN. The percentage difference for deflection was 9.3 %, which validated the finite element model. Fig. 19 shows model EN-A's moment–rotation curves and the experiment by Bahrami et al. (3) at ambient temperature. It is observed that the curves showed a good agreement between them. Model EN-A had a higher stiffness compared to the experiment. The percentage difference for rotation was 8.5%.

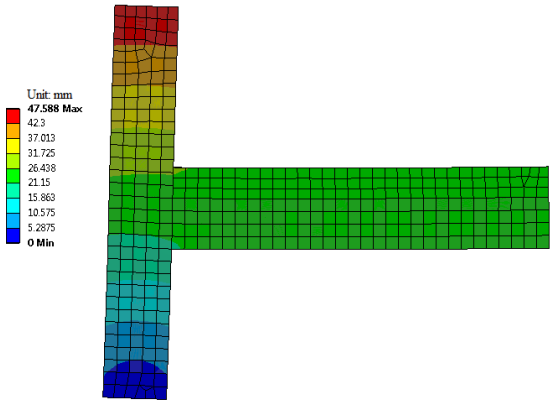

Fig. 17 Deflection of model EN-A

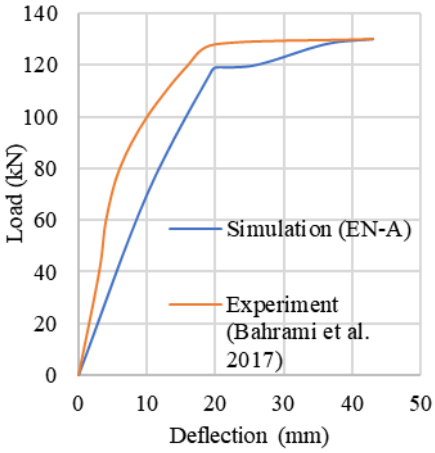

Fig. 18 Load – deflection curves of model EN-A and experiment [3] at ambient temperature

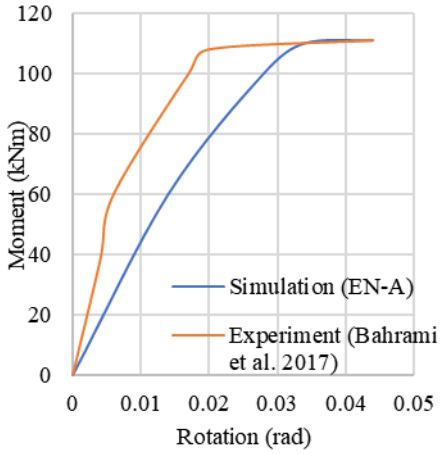

Fig. 19 Moment - rotation curves of model EN-A and experiment [3] at ambient temperature

5.3.2 High temperature

For model validation, Fig. 20 shows the load-deflection curves of model EN-HT and the experiment by Radzi (13) at high temperatures. Table 6 compares the load–deflection ratio between the model CN-HT and the experiment by Radzi (13). The load–deflection ratio showed a difference of 24.2%. This significance was due to the non-uniformity of sample dimensions and different test setups in the study by Radzi (2023) (13). The load in the simulation was a lateral applied at the column. The load in the experiment was a vertically applied beam.

Table 6. Load – deflection curves of model CN-HT and experiment (13) at high temperature

Items	EN-HT [A]	Experiment (13) [B]	Differences [B] – [A]	Percentage Difference (%)
Load (kN)	92	63	29	31.52
Deflection (mm)	60.1	54.3	5.8	9.7

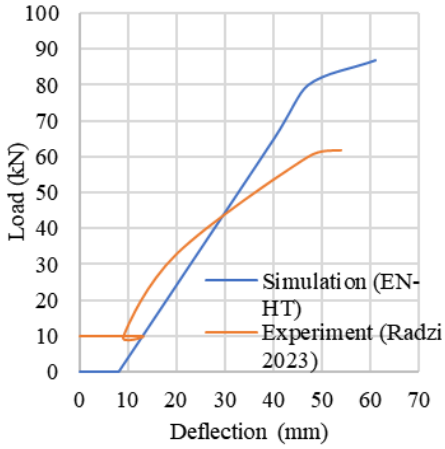

Fig. 20 Load – deflection curves of model EN-HT and experiment [9] at high temperature

5.3.3 Comparison of Ambient and High Temperature

Fig. 21 shows the load-deflection curves of models EN-A and EN-HT. The maximum deflection for model EN-A was 43.04 mm with a maximum load of 130 kN. The maximum deflection for model CN-HT was 59.51 mm with a maximum load of 94.68 kN. Observation showed that CN-A was performing better than CN-HT. The thermal percentage deterioration of load and displacement is 26.9 % and 27.9 %, respectively.

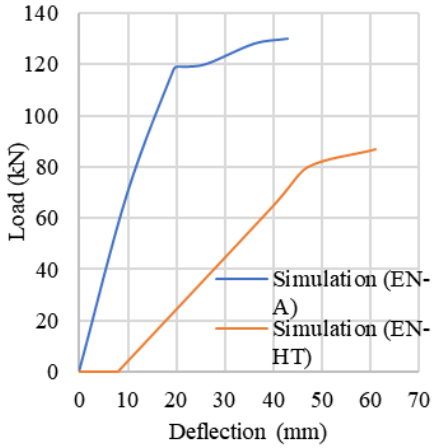

Fig. 21 Load – deflection curves of model EN-A and EN-HT

6. Results Comparison

Table 7 lists the validation of finite element models based on the previous experiment at ambient temperature (3,17,18) and high temperature (13). The percentage difference for finite element models at ambient temperature was less than 10 %, which validated the finite element model. However, the percentage difference for finite element models at high temperatures exceeded 10 %, which were not validated the finite element model. This significant difference was due to the non-uniformity of sample dimensions and different

test setups in the study by Radzi (2023) (13). The load in the simulation was a lateral applied at the column. The load in the experiment was vertically applied to the beam.

Table 7. Validation of finite element models

Connections	Validation with Previous Experiment	
	Ambient [3], [11], [12]	High Temperature [9]
Concrete corbel	√	×
Concrete nib	√	×
Inverted E steel nib	√	×

√ = Validated, percentage difference less than 10%
× = Not validated, percentage difference more than 10%

Table 8 lists the comparison of thermal percentage deterioration based on load and deflection values at high temperatures compared to ambient temperatures. Concrete nib recorded the most significant thermal percentage deterioration (32.1 % and 57.4 %) compared to concrete corbel (22.4 % and 11.52 %) and inverted E steel nib (26.9 % and 27.9 %). The concrete corbel and inverted E steel nib models had an additional strength factor by the vertical dowel reinforcement and the stiffness of the E steel component compared to the concrete nib.

Table 8. Thermal percentage deterioration of finite element models

Connections	Thermal Percentage Deterioration (%)	
	Load	Deflection
Concrete corbel	22.4	11.52
Concrete nib	32.1	57.4
Inverted E steel nib	26.9	27.9

7. Conclusions

Based on the results of nonlinear coupled thermal-structural analysis using ANSYS Workbench on three precast connection models presented in this paper, the following conclusions can be drawn on the nonlinear coupled thermal-structural analysis of precast concrete beam-to-column connections:

- Finite element models CC-A, CN-A, and EN-A at ambient temperature were validated with a less than 10% percentage difference. However, finite element models CC-HT, CN-HT, and EN-HT at high temperatures were not verified due to the percentage difference exceeding 10 % due to the non-uniformity of sample dimensions and different test setups between the simulation and the experimental study by Radzi (2023) (13).
- At ambient temperatures, the finite element models CC-A dan EN-A have a higher stiffness than the experimental sample. However, the CN-A finite element model has a lower stiffness than the experimental sample.
- At high temperatures, the concrete nib recorded the most significant thermal percentage deterioration (32.1 % and 57.4 %) compared to concrete corbel (22.4 % and 11.52 %) and inverted E steel nib (26.9 % and 27.9 %). The concrete corbel and inverted E steel nib models had an additional strength factor by the vertical dowel reinforcement and the stiffness of the E steel component compared to the concrete nib.
- The post-fire effects on connection elements in precast structures such as bearing pads, grouting, and welding influenced the thermal percentage deterioration.

Fire-damaged to beam-to-column connections reduce the rigidity of the beam structure and the integrity between the beam end and the column connection.

- The validation result of nonlinear coupled thermal-structural analysis executed using ANSYS Workbench gives good efficiency for predicting the fire performance of precast concrete corbel beam-to-column connections at high temperatures.

Conflicts of Interest

The authors declare that they have no known conflict of financial interests or personal relationships that could have appeared to influence the work reported in this paper. This work was supported by the Universiti Kebangsaan Malaysia Research University Grant (grant no. GUP-2018-027).

References

[1] Hollý I, Harvan I. Connections in precast concrete elements. Key Eng Mater. 2016;691:376-87. https://doi.org/10.4028/www.scientific.net/KEM.691.376
[2] Fatema T. Study on Connection Between Precast Concrete Beam and Cast-in-Situ Column in Prefabricated Building Frames. J Eng Appl Sci. 2006;1(1):33-8.
[3] Bahrami S, Madhkhan M, Shirmohammadi F, Nazemi N. Behavior of two new moment resisting precast beam to column connections subjected to lateral loading. Eng Struct [Internet]. 2017;132:808-21. https://doi.org/10.1016/j.engstruct.2016.11.060
[4] European Committee For Standardization. Eurocode 2: Design of concrete structures - Part 1-2: General rules - Structural fire design. Vol. 1. 2011.
[5] Eid F, Heiza K, Elmahroky M. Behavior and Analysis of Reinforced Self-Compacted Concrete Beam Column Connection Subjected to Fire. Am J Sci Eng Technol. 2017;
[6] Kien DD, Trinh D Van, Toan KT, Danh LB. Fire Resistance Evaluation of Reinforced Concrete Structures. Proc 2020 5th Int Conf Green Technol Sustain Dev GTSD 2020. 2020;588-92. https://doi.org/10.1109/GTSD50082.2020.9303102
[7] Yakudima AG et al. Impact of Fire on Steel Reinforcement In Reinforced Concrete Structures. 2015;5(10):46.
[8] Teja CS, Moturu TS, Yaswanth Kumar G, Khan HA, Kumar GY, Khan HA. Effect of Fire on Prefabricated Concrete Beam Column Connections. Int J Recent Technol Eng. 2019;8(2):1433-6. https://doi.org/10.35940/ijrte.B2092.078219
[9] ASTM. ASTM E119-07: Standard methods of fire test of building construction and materials. ASTM - Am Soc Test Mater. 2007;1-21.
[10] ISO. Fire-resistance tests - Elements of building construction - Part 2: Requirements and recommendations for measuring furnace exposure on test samples. ISO 834-2. Geneva; 1999.
[11] Mao CJ, Chiou YJ, Hsiao PA, Ho MC. Fire response of steel semi-rigid beam-column moment connections. J Constr Steel Res. 2009; https://doi.org/10.1016/j.jcsr.2008.12.009
[12] Mahale HD, Kandekar SB. Behaviour of steel structure under the effect of fire loading. Int J Eng Res Appl www.ijera.com [Internet]. 2016;6(5):42-6. Available from: www.ijera.com
[13] Radzi NAM. Kelakuan Terma dan Struktur Sambungan Rasuk ke Tiang Konkrit Pratuang Luaran Pada Suhu Tinggi. Ph.D Thesis. Ph.D Thesis, Universiti Kebangsaan Malaysia; 2023.
[14] Radzi NAM, Hamid R, Mutalib AA, Kaish ABMA. A Review of Precast Concrete Beam-to-Column Connections Subjected to Severe Fire Conditions. Adv Civ Eng [Internet]. 2020;2020:1-23. https://doi.org/10.1155/2020/8831120

[15] Radzi NAM, Hamid R, Mutalib AA, Kaish ABMA. A Review of the Structural Fire Performance Testing Methods for Beam-to-Column Connections. Adv Civ Eng. 2021;2021:1-36. https://doi.org/10.1155/2021/5432746
[16] Dzolev I, Cvetkovska M, Ladjinovic D, Radonjanin V, Raseta A. Fire Analysis of a Simply Supported Reinforced Concrete Beam Using Ansys Workbench. 2016;(September).
[17] Rahman ABA, Ghazali AR, Abd. Hamid Z. Comparative study of monolithic and precast concrete beam-to-column connections. Malaysian Constr Res J. 2008;2(1):42-55.
[18] Mokhtar R, Ibrahim Z, Jumaat MZ, Hamid ZA, Hazim A, Rahim A. Behaviour of Semi-rigid Precast Beam-to-column Connection Determined Using Static and Reversible Load Tests. Measurement [Internet]. 2020;108007. https://doi.org/10.1016/j.measurement.2020.108007
[19] Radzi NAM, Muniandy S, Ismasafie FS, Hamid R. Nonlinear Coupled Thermal-Structural Analysis of Monolithic and Precast Concrete Corbel Beam-to-Column Connection. In: Proceedings ofThe 17th East Asian-Pacific Conference on Structural Engineering and Construction, 2022. Springer; 2023. p. 581-196. https://doi.org/10.1007/978-981-19-7331-4_47
[20] ANSYS Inc. Mechanical APDL Element Reference. Vol. 15317. 2010. 1-1416 p.
[21] Tjitradi D, Eliatun E, Taufik S. 3D ANSYS Numerical Modeling of Reinforced Concrete Beam Behavior under Different Collapsed Mechanisms. Int J Mech Appl [Internet]. 2017;7(1):14-23. Available from: http://journal.sapub.org/mechanics
[22] Elshorbagy M, Abdel-Mooty M. The coupled thermal-structural response of RC beams during fire events based on nonlinear numerical simulation. Eng Fail Anal. 2020. https://doi.org/10.1016/j.engfailanal.2019.104297